Spectral modulation observed in Chl-*a* by ultrafast laser spectroscopy

Juan Du,[1,2,3,7] Kazuaki Nakata,[4] Yongliang Jiang,[1,3] Eiji Tokunaga,[4] and Takayoshi Kobayashi,[1,3,5,6,8]

[1]*Advanced Ultrafast Laser Research Center, and Department of Engineering Science, Faculty of Informatics and Engineering, University of Electro-Communications, 1-5-1, Chofugaoka, Chofu, Tokyo 182-8585, Japan*
[2]*State Key Laboratory of High Field Laser Physics, Shanghai Institute of Optics and Fine Mechanics, Chinese Academy of Sciences, Shanghai 201800, China*
[3]*Core Research for Evolutional Science and Technology (CREST), Japan Science and Technology Agency, 4-1-8 Honcho, Kawaguchi, Saitama 332-0012, Japan*
[4]*Department of Physics, Faculty of Science, Tokyo University of Science, 1-3 Kagurazaka, Shinjuku, Tokyo 162-8601, Japan*
[5]*Institute of Laser Engineering, Osaka University, 2-6 Yamada-oka, Suita, Osaka 565-0871, Japan*
[6]*Department of Electrophysics, National Chiao Tung University, 1001 Ta Hsueh Rd., Hsinchu 30010, Taiwan*
[7]*dujuan@ils.uec.ac.jp*
[8]*kobayashi@ils.uec.ac.jp*

Abstract: Broadband real-time dynamic vibronic coupling in Chl-*a* were experimentally studied using few cycle laser pulses of 6.8fs duration and a 128-channnel lock-in amplifier. Thanks to the extreme temporal resolution benefitting from the ultrashort laser pulse, the real-time modulation of the electronic transition energy induced by the molecular vibrations were calculated by the time dependent first moments of the bleaching band. The transition energy was found to be modulated periodically with the same frequencies of molecular vibration found in the Fourier amplitude spectrum of the difference absorbance real-time traces. This was interpreted to be due to the difference in the effective transition energy associated with the wavepacket motion induced by the equilibrium positions of potential curves between the ground state and the excited state. Using the values, Huang–Rhys factors for several vibrational modes involved in the spectral modulation at the room-temperature have been determined.

OCIS codes: (140.7090) Ultrafast lasers; (300.6500) Spectroscopy, time-resolved; (320.2250) Femtosecond phenomena; (160.1435) Biomaterials.

References and links

1. K. K. Rebane and R. A. Avarmaa, "Sharp line vibronic spectra of chlorophyll and its derivatives in solid solutions," Chem. Phys. **68**(1–2), 191–200 (1982).
2. R. J. Platenkamp, H. J. Den Blanken, and A. J. Hoff, "Single-site absorption spectroscopy of pheophytin-a and chlorophyll-a in a n-octane matrix," Chem. Phys. Lett. **76**(1), 35–41 (1980).
3. M. Rätsep, J. Linnanto, and A. Freiberg, "Mirror symmetry and vibrational structure in optical spectra of chlorophyll a," J. Chem. Phys. **130**(19), 194501 (2009).
4. J. R. Diers, Y. Zhu, R. E. Blankenship, and D. F. Bocian, "Qy-excitation resonance Raman spectra of chlorophyll a and bacteriochlorophyll c/d aggregates: effects of peripheral substituents on the low-frequency vibrational characteristics," J. Phys. Chem. **100**(20), 8573–8579 (1996).
5. C. Zhou, J. R. Diers, and D. F. Bocian, "Q_y-excitation resonance Raman spectra of chlorophyll a and related complexes: normal mode characteristics of the low-frequency vibrations," J. Phys. Chem. B **101**(46), 9635–9644 (1997).
6. J. K. Gillie, G. J. Small, and J. H. Golbeck, "Nonphotochemical hole burning of the native antenna complex of photosystem I (PSI-200)," J. Phys. Chem. **93**(4), 1620–1627 (1989).
7. A. Pascal, E. Peterman, C. Gradinaru, H. van Amerongen, R. van Grondelle, and B. Robert, "Structure and interactions of the chlorophyll a molecules in the higher plant Lhcb4 antenna protein," J. Phys. Chem. B **104**(39), 9317–9321 (2000).
8. A. Shirakawa, I. Sakane, and T. Kobayashi, "Pulse-front-matched optical parametric amplification for sub-10-fs pulse generation tunable in the visible and near infrared," Opt. Lett. **23**(16), 1292–1294 (1998).
9. A. Baltuška, T. Fuji, and T. Kobayashi, "Visible pulse compression to 4 fs by optical parametric amplification and programmable dispersion control," Opt. Lett. **27**(5), 306–308 (2002).

#153616 - $15.00 USD Received 30 Aug 2011; revised 22 Sep 2011; accepted 23 Sep 2011; published 25 Oct 2011

10. K. Okamura and T. Kobayashi, "Octave-spanning carrier-envelope phase stabilized visible pulse with sub-3-fs pulse duration," Opt. Lett. **36**(2), 226–228 (2011).
11. A. H. Zewail, "Laser femtochemistry," Science **242**(4886), 1645–1653 (1988).
12. T. Kobayashi, T. Saito, and H. Ohtani, "Real-time spectroscopy of transition states in bacteriorhodopsin during retinal isomerization," Nature **414**(6863), 531–534 (2001).
13. H. H. Strain and W. A. Svec, "Extraction, separation, estimation and isolation of the chlorophylls," in *The Chlorophylls*, L. P. Vernon and G. R. Seeley, eds. (Academic, 1966), pp. 21–26.
14. J. Du, T. Teramoto, K. Nakata, E. Tokunaga, and T. Kobayashi, "Real-time vibrational dynamics in chlorophyll a studied with a few-cycle pulse laser," Biophys. J. **101**(4), 995–1003 (2011).
15. G. Korn, O. Dühr, and A. Nazarkin, "Observation of Raman self-conversion of fs-pulse frequency due to impulsive excitation of molecular vibrations," Phys. Rev. Lett. **81**(6), 1215–1218 (1998).
16. T. Kobayashi and A. Yabushita, "Transition-state spectroscopy using ultrashort laser pulses," Chem. Rec. **11**(2), 99–116 (2011).
17. T. Kobayashi, J. Zhang, and Z. Wang, "Non-Condon vibronic coupling of coherent molecular vibration in MEH-PPV induced by a visible few-cycle pulse laser," New J. Phys. **11**(1), 013048 (2009).
18. S. Quan, F. Teng, Z. Xu, T. Zhang, L. Qian, D. Liu, Y. Hou, and Y. Wang, "Temperature effects on photoluminescence of poly[2-methoxy-5-(20-ethyl-hexyloxy)-1,4-phenylene vinylene]," Mater. Lett. **60**(9–10), 1134–1136 (2006).

1. Introduction

Chlorophyll *a* (Chl-*a*) plays an essential role in the energy transfer and charge separation in the photosynthetic unit, hence Chl-*a* and Chl-containing proteins have been extensively studied [1–3].Among these studies, applications of laser pulses with durations from several tens to 100fs have been reported. On the other hand, the vibrational structure of Chl-*a* has been obtained by resonance Raman spectroscopy, spectral hole-burning, and fluorescence line-narrowing techniques, respectively [3–7]. However, the vibrational information of its most interesting Q_y-band is usually studied at very low temperature (~4K) due to the temperature requirement of these vibrational methods and disturbance by intense fluorescence in Chl-*a* solution. Vibrational result at physiologically relevant temperature has not been elucidated, and no study has yet been reported on the coherent molecular vibration induced by impulsive excitation with a sufficiently short pulse.

With the development of the ultrashort pulse laser techniques, few-cycle pulses in the visible and near-infrared ranges have been generated [8,9]. Among these methods, the noncollinear phase-matched optical parametric amplification (NOPA) technique has attracted great interests. Using this method, sub-5-fs pulses in the visible spectral range have been generated by our group [8,9]. Recently, pulse with duration as short as 2.4fs with carrier envelope phase stabilization has been realized [10].These ultrashort pulse lasers make it possible to observe the real-time electronic, phonon, and vibrational dynamics in various molecular systems, which has provide microscopic insights into bulk materials, molecules, and chemical and biochemical reaction processes [11,12]

In the present study, we used a 6.8 fs laser for broad-band pump-probe real-time vibrational spectroscopy to obtain both electronic relaxation and vibrational dynamics of Chl-*a* at physiologically relevant temperature. Due to the broad probe wavelength extending from 539 nm to 738 nm, the dynamics of the vibrational modes coupled to the electronic transition of the whole Q_y-band in Chl-*a* has been detected. The modulations of the electronic transition energy have been observed and determined, and been explained in terms of Huang–Rhys factors.

2. Experimental method and material

The Chl-*a* sample was extracted from spinach leaves and subsequently purified using chromatographic method [13]. The solvent used here is a mixture of petroleum ether and 2-propanol with a ratio of 100:5. The stationary absorption curve and the fluorescence spectra of Chl-*a* solution were shown in Fig. 1. In the real-time pump-probe experiment, the Chl-*a* sample is placed in a 0.5 mm fused silica flow cell with 1.25 thick mm window on both sides.

The seed and pump of our NOPA system were generated from the same commercial CPA laser (Spectra Physics, Spitfire). The white light seed generated from a 1mm sapphire was amplified in a 1mm thick BBO crystal, and the amplified broadband pulse was compressed by

#153616 - $15.00 USD Received 30 Aug 2011; revised 22 Sep 2011; accepted 23 Sep 2011; published 25 Oct 2011

a pair of Brewster angle prisms and chirp mirrors. The pulse duration was measured to be 6.8fs after the front sample cell window. The output spectral range extends from 539nm to 738nm (Fig. 1). Both the pump and probe of our spectroscopy experiment were generated from the same NOPA pulse, and the pulse energies were 42 and 6 nJ, respectively.

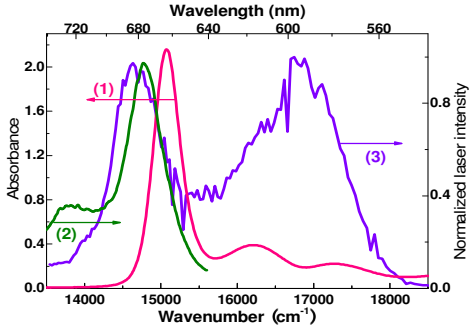

Fig. 1. The absorption spectrum(1), fluorescence spectrum (2) of Chl a, and the NOPA laser spectrum (3).

We applied the combination of a polychromator and a multi-channel lock-in amplifier (Signal Recovery, Model 7210) to detect the signal. After the sample, the probe pulses were dispersed by the polychromator (300 grooves/mm, 500 nm blazed) and guided to the 128 avalanche photodiodes by a fiber bundle. The spectral resolution of the total system was 1.5 nm. The wavelength dependent absorbance difference was measured at delay times from −200 to 1800 fs with 0.8 fs step. All experiments were performed at a constant temperature (293K).

3. Results and discussion

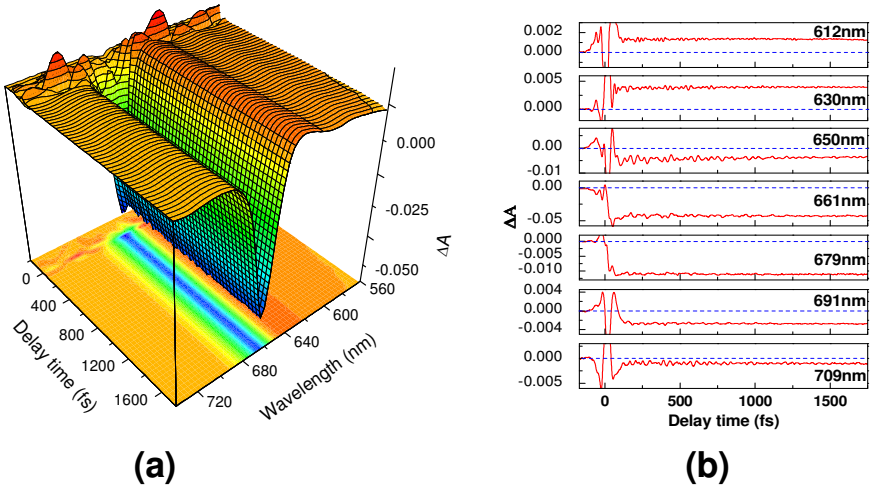

Fig. 2. (a) Birds-eye view of the time-resolved difference absorption spectra of Chl-a. (b) Real-time traces at seven typical wavelengths. The dashed lines represent ΔA = 0.

Figure 2 shows the three dimensional plot of the time-resolved difference absorption curves of Chl-*a* as functions of the probe wavelength and the delay time. The negative Δ*A* signal is due to the increase of the transmitted probe light intensity caused by the absorption bleaching owing to the ground state depletion and/or stimulated emission; whereas the positive one represents the contribution from the induced absorption. The most intense negative peak signal is located around the $Q_y(0,0)$ transition peak at 664 nm, and shows an asymmetric profile. This can be explained in the following way that the transient signal observed at probe wavelength longer than 664nm is due to the mixed contribution of both the ground state

#153616 - $15.00 USD Received 30 Aug 2011; revised 22 Sep 2011; accepted 23 Sep 2011; published 25 Oct 2011

bleaching (BL), the stimulated emission (SE) and possible induced absorption (IA) from Q_y state to even higher excited states, while the ΔA at probe wavelength shorter than 664nm is dominated by the BL and the IA.

It is noteworthy that the time dependent ΔA signal in Fig. 2(b) shows predominant periodic modulation due to molecular vibration. To gain a better understanding of the vibronic coupling mechanisms, the vibrational mode frequencies and its corresponding amplitudes have been evaluated by the fast Fourier transform (FFT) analysis, which was performed after subtractions of averaging data over 200 fs from raw data to remove the slow decay dynamics due to dynamics in the relevant electronic states. Figure 3 depicts the three-dimensional plot of the Fourier power against the molecular vibration frequency and probe photon energy (wavelength). There are two main vibrational bands. The weaker one is located around 14100cm^{-1} (709nm) and has been assigned to the vibronic coupling to the IA from Q_y state to an even higher state [14]. The stronger one is near the ground state absorption peak of Chl-*a*. More than 25 vibrational modes have been observed in this spectral range. It is noteworthy that the high-frequency modes (>700cm^{-1}) in this vibrational band show clear side-band signals, which are distributed as the linear function (slope K = 1) of their own vibrational frequencies. The spectral distributions of the side-band amplitudes and phases could be discussed in terms of energy exchange intermediated by vibrational coherence [14]. In the following, we will concentrate on the discussion of the real-time spectral modulation effect induced by the observed molecular vibrations.

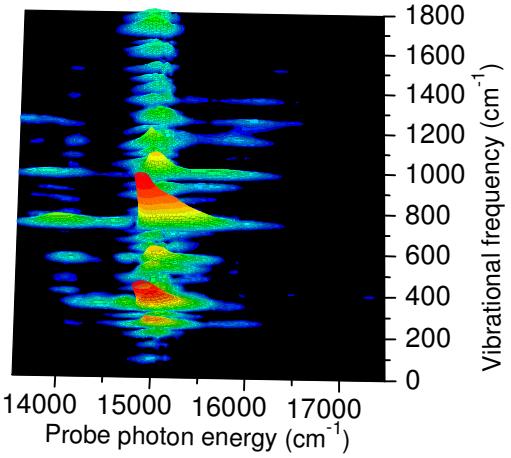

Fig. 3. Three-dimensional plot of FT amplitude spectra of the pump-probe signal.

Figure 4(a) shows the integrated signal intensity in the whole range of the Gaussian-like strong Q-band from 14503 cm^{-1} (689.5 nm) to 15366 cm^{-1} (650.5nm), $\Delta A^I(t) = \int_Q \Delta A(\omega,t)\, d\omega$ (zeroth moment) calculated with a step of 0.8 fs representing the total electronic transition probability of the Q-band. The electronic transition energy at each delay time can be monitored by the first-moment expressions of

$$\varpi(t) = \int_Q \Delta A(\omega,t) \bullet \omega \; d\omega \,/ \int_Q \Delta A(\omega,t) \; d\omega \qquad (1)$$

As shown in Fig. 4(c), starting from the initial value of 14980 cm^{-1}, the center probe photon energy shows highly delay-time dependent modulation, suggesting that the time-resolved ΔA spectra undergo non-negligible spectral shift at different delay times. Its corresponding FT power spectra are as shown in Fig. 4(d). There are five main modes clearly appearing with the frequency of 259, 346, 565, 743, and 982 cm^{-1}. The contribution of each vibrational mode to the spectral shift can be determined by a simple simulation of a linear combination of five functions expressed by

#153616 - $15.00 USD Received 30 Aug 2011; revised 22 Sep 2011; accepted 23 Sep 2011; published 25 Oct 2011

$$\delta\omega_{simu}(t) = \sum_i \delta\omega_{vi} \exp(-t/\tau_{vi}) \cos(\omega_{vi} t + \varphi_i), \quad (i = 1, 2, ..., 5) \tag{2}$$

Here, ω_{vi} is the vibrational frequency of each mode; τ_{vi} is the vibrational dephasing time; φ_i is the initial phase, respectively. The corresponding spectral modulation $\delta\omega_{vi}$ are calculated to be 2.83, 8.72, 4.80, 10.81, and 3.44 cm^{-1} for 259, 346, 565, 743, and 982 cm^{-1} mode, respectively.

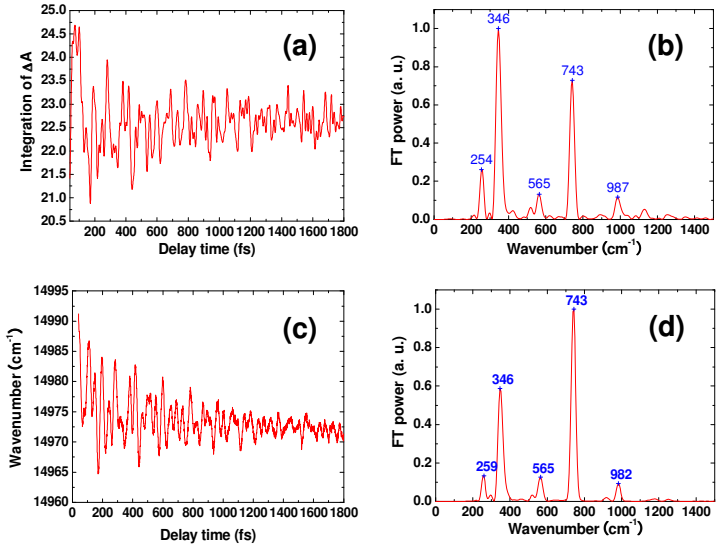

Fig. 4. Probe delay time dependence of the integrated ΔA signal intensity in the Q band (a), the electronic transition energy (c), and their corresponding FT power spectra (b) and (d), respectively.

In the following discussion, we will concentrate on the explanation of this spectral modulation. As we noticed that all the vibrational modes appearing in Fig. 4(d) have frequencies lower than 1000cm^{-1}, and these modes have been assigned to vibrations of the tetrapyrrole skeleton and deformations of the peripheral substituent groups [4,5], which are easily to be involved in the molecular structure change in the Chl-*a* much more effectively than those with higher frequency. So at first glance, this spectral modulation might be considered to be caused by molecular vibration phase modulation (MPM) mechanism, i.e. the propagation of the probe pulse is modified through the delay-time dependent variation of refractive index induced by the molecular vibrations excited by the pump pulse [15]. Especially, the modes of 346 and 743 cm^{-1} undergo much stronger vibronic coupling as shown in Fig. 3. Therefore the refractive index changes caused by their vibrational motions are expected to be much more intense than by other modes. However, as compared the spectral modulation contributed from single Chl-a molecule was calculated to be 10^3 times larger than that one due to single SF_6 molecule. This difference is too large to be explained by the difference in the molecular structure. Then we need go back to the original data of $\Delta A(\omega)$ spectra to find the real reason. In pump-probe experiment, the modulation of the absorbance change ($\delta\Delta A(\omega)$) can be expressed as a function of the probe frequency ω [16]

$$\begin{aligned} \delta\Delta A(\omega,t) &= \Delta A(\omega,t) - \overline{\Delta A(\omega,t)} \\ &\cong \left(\frac{\delta(\mu_{QG}{}^2(t))}{\mu_{QG}{}^2(t)} \Delta A(\omega,t) + \delta\omega(t) \frac{d\Delta A(\omega,t)}{d\omega} + \delta\Delta\omega(t) \frac{d^2\Delta A(\omega,t)}{d\omega^2}\right) \cos(\omega_v t + \phi) \end{aligned} \tag{3}$$

Here, μ is the transition dipole moment, $\delta\omega$ is the change of the electronic transition energy, and $\delta\Delta\omega$ is the change in the bandwidth ΔA spectrum. The first term in Eq. (3)

#153616 - $15.00 USD Received 30 Aug 2011; revised 22 Sep 2011; accepted 23 Sep 2011; published 25 Oct 2011

represents the modulation of m of the relevant electronic transition, which is zero when the Condon approximation is satisfied. If we apply the conventional Franck–Condon-type wave packet in the excited state to explain the origin of this molecular vibration, the integrated intensity of the absorbance change covering the relevant electronic state transition range will not change during the wave-packet motion [16]. In the case of Chl-*a*, it is not constant but highly modulated as shown in Fig. 4(a), which indicates that the vibrational modes shown in Fig. 4(b) can be classified as non-Condon type or the Raman type which can explain the intensity modulation through energy exchange between the laser, Stokes, and anti-Stokes field intermediated by the molecular vibrations. The second term corresponding to the case when the potential minimum is displaced between ground state and excited state. If the displacement is small, the probe wavelength dependence of vibrational amplitude resulted from this term will be related to the first derivative of the corresponding transition spectrum. As we know that the Huang-Rhys factors of Chl-*a* are significantly small, the first derivative type contribution to the $\delta\Delta A(\omega)$ spectra should not be neglected here. The third term in Eq. (3) takes effect when there is no displacement between the ground and excited states. It is not the case of Chl-*a* molecule, so we did not calculate this term here.

Based the description above, if the electronic transition energy change can be discussed in terms of the difference in the equilibrium positions of potential curves between the ground state and the excited state, the Huang–Rhys factor *S* for each vibrational mode can be calculated to be $S_{259} = 0.011$, $S_{346} = 0.025$, $S_{565} = 0.008$, $S_{743} = 0.015$, and $S_{982} = 0.004$ by $\delta\omega_{vi} / \omega_{vi}$ based on the calculation result of Eq. (2). Except the value obtain for the weakest mode at 982cm^{-1}, all the other factors are of the same order with those reported in [6]. The slight difference in the two series values may due to different experimental temperature and different environment of Chl-*a*, because the hole burning experiment in [6] was performed at 1.6K in a light-harvesting complex of photosystem I (PSI-200). To verify this assumption, we calculated the Huang–Rhys factors for the vibrational modes in MEH-PPV [17]. And the result are $S_{961} = 0.232$, $S_{1278} = 0.201$, $S_{1315} = 0.187$, and $S_{1587} = 0.175$, respectively. Then the average Huang–Rhys factor can be determined to be 0.4, which is in good agreement with the reported value of 0.51 [18]. Even though the spectral modulation size in MEH-PPV are remarkable large (~250cm^{-1}) [17] in contrast to ~10 cm^{-1} in the case of Chl-*a,* it is reasonable to attribute them to the same mechanism if their Huang–Rhys factors and involved vibrational frequencies are taken into consideration.

4. Conclusion

We used a 6.8fs laser as the light source of the broadband real-time vibrational spectroscopy to study the coherent molecular vibration in Chl-*a*. Due to advantages of ultrafast excitation and broadband detection, the probe wavelength dependence of the vibration amplitude in Chl-*a* was detected with high sensitivity. The electronic transition energy change has been calculated and explained in terms of the difference in the equilibrium positions of potential curves between the ground state and the excited state. Due to the temperature limitation of conventional vibrational spectroscopic techniques in the study on Chl-*a* and the complexity of the temperature dependent characteristic of Chl-*a*, its Q-band vibrational information at physiologically relevant temperature is always scarce and desirable. The room-temperature information obtained here is promising to reveal the hidden features of Chl-*a* at physiologically relevant temperature directly.

Acknowledgments

This work was supported by the Core Research for Evolutional Science and Technology program of the Japan Science and Technology Agency, National Science Council of the Republic of China, Taiwan (NSC No. 98-2112-M-009-001-MY3), and a grant from the Ministry of Education, Aiming for Top University Program at National Chiao-Tung University. A part of this work was performed under the joint research project of the Institute of Laser Engineering, Osaka University under contract No. A3-01.

#153616 - $15.00 USD Received 30 Aug 2011; revised 22 Sep 2011; accepted 23 Sep 2011; published 25 Oct 2011